Field Performance and Thermal-Electrical Mismatch Mechanism of Curved CIGS BIPV Modules: An Outdoor Experimental Study

Jun Wang , Xinyi Tian , Mingjun Jiang , Guodong Lu , Jie Ji , Haitao Wang , Qiansheng Fang *

Posted Date: 9 April 2026

doi: 10.20944/preprints202604.0480.v1

Keywords: flexible CIGS module; curved bending forms; outdoor experiment; photoelectric mismatch mechanism; thermal distribution

 doi:10.20944/preprints202604.0480.v1

Article

Field Performance and Thermal-Electrical Mismatch Mechanism of Curved CIGS BIPV Modules: An Outdoor Experimental Study

Jun Wang [1,2,3,4], Xinyi Tian [5,6], Mingjun Jiang [7,8], Guodong Lu [5,6], Jie Ji [5,6], Haitao Wang [1] and Qiansheng Fang [2,3,4,*]

[1] School of Environment and Energy Engineering, Anhui Jianzhu University, Hefei, Anhui, China
[2] Anhui Province Key Laboratory of Intelligent Building and Building Energy-saving, Anhui Jianzhu University, Hefei, Anhui, China
[3] Anhui Institute of Strategic Study on Carbon Emissions Peak and Carbon Neutrality in Urban-rural Development, Anhui Jianzhu University, Hefei, Anhui, China
[4] School of Electrics and Information Engineering, Anhui Jianzhu University, Hefei 230601, China
[5] Department of Thermal Science and Energy Engineering, University of Science and Technology of China, Hefei 230026, China
[6] Key Laboratory of Solar Thermal Conversion of Anhui Province, Hefei, 230026, Anhui, China.
[7] School of Architecture & Urban Planning, Anhui Jianzhu University, Hefei, Anhui, China
[8] Key laboratory of Huizhou Architecture in Anhui Province, Anhui Jianzhu University, Hefei, Anhui, China
[9] School of Electrics and Information Engineering, Anhui Jianzhu University, Hefei, China.
* Correspondence: fqs@ahjzu.edu.cn; Telephone: +86-0551-63607346

Abstract

Flexible photovoltaic modules offer an innovative approach for Building Integrated Photovoltaics (BIPV) on non-planar envelopes. However, the dynamic outdoor environment aggravates the photoelectric mismatch mechanism caused by complex curved geometries. This study experimentally investigates the outdoor experimental investigation into the dynamic electrical and thermal performance of large-scale curved CIGS modules equipped with bypass diodes. Six representative configurations—flat, length-convex(lgvx), length-concave(lgcv), width-convex(wdvx), width-concave(wdcv), and wavy—were continuously monitored under real weather conditions in Hefei, China. The results indicate that while flat modules maintain the highest daily energy yield (453.32 Wh) , the wdvx in longitudinal direction exhibits exceptional adaptability, achieving an average Performance Ratio (PR) of 91.46% and outperforming the flat type during low solar altitude periods in the day. Infrared thermal imaging reveals significant temperature gradients driven by the mismatch effect, with the lgcv module reaching a peak temperature of 65.88°C. Furthermore, the I-V characteristic curves demonstrate that non-uniform self-shading triggers bypass diode activation, resulting in severe step-like current drops and multiple power peaks in concave and wavy shapes. These findings offer crucial practical guidelines for optimizing cell layout and thermal management in curved BIPV envelops.

Keywords: flexible CIGS module; curved bending forms; outdoor experiment; photoelectric mismatch mechanism; thermal distribution

1. Introduction

With rapid urbanization and the drive toward carbon neutrality, building energy consumption, which accounts for a substantial portion of global energy use, has become a critical focus. In 2024, the building sector represented the largest share, accounting for 34% of total global energy consumption and 37% of the associated CO_2 emissions. According to the China Association of Building Energy

 doi:10.20944/preprints202604.0480.v1

Efficiency (CABEE), carbon emissions from building operations in China reached 2.47 billion tonnes in 2024, contributing to more than 22.10% of the country's total carbon emissions[1].

Building-Integrated Photovoltaics (BIPV) serve as a primary strategy to mitigate building operational emissions by transforming passive envelopes into active power generators. While standard planar PV modules are widely commercialized, contemporary architectural designs increasingly favor magnificent spatial curved structures for both aesthetic appeal and structural efficiency. However, the rigid nature of traditional crystalline silicon panels severely limits their application on these complex geometries. Consequently, thin-film technologies, particularly Copper Indium Gallium Selenide (CIGS) modules deposited on flexible stainless steel substrates, have emerged as a highly promising BIPV solution. Distinct from glass-based semi-transparent alternatives, these opaque, stainless steel-based CIGS modules offer exceptional mechanical robustness, lightweight properties, and seamless morphological adaptability. These characteristics make them uniquely suited for large-span curved roofs and complex non-planar envelopes, including BIPV roofs[2, 3], walls[4, 5], windows[6-8], and shadings devices[9, 10], while ensuring perfect conformal integration without compromising the architectural design.

As shown in Fig.1a-c. In China, the practical implementation of seamlessly integrating PV modules into curved buildings has seen exemplary progress across various architectural styles. In curved BIPV systems, conventional glass-based modules suffer from a relatively large self-weight, restricting their broad application. While small-scale corrugated PV tiles can directly replace traditional roofing materials in residential buildings, adapting rigid modules to large-scale curved surfaces typically requires parameterizing and tessellating the envelope, subsequently integrating planar PV modules within each discrete facet. This conventional approach inevitably necessitates complex support structures and imposes stringent load-bearing requirements. In contrast, flexible CIGS modules bypass these structural limitations, offering a lightweight and conformal solution. Furthermore, curved structural integration allows for a larger active PV area compared to planar installations, thereby increasing the total installed capacity[11].

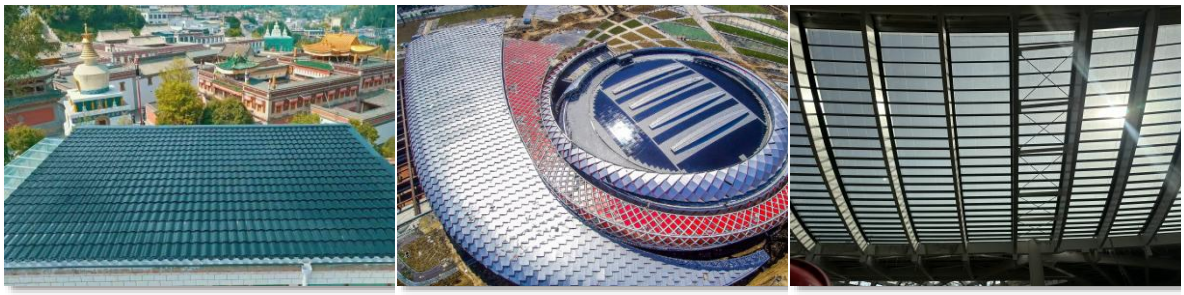

(a)Curved CIGS Roof tiles in Xining Traditional Building

(b) Curved CIGS Roof in Bengbu Olympic Sports Center

(c) Curved CdTe translucent Roof in Hefei Xinqiao Airport

Figure 1. Photos of buildings with curved PV modules.

However, the geometric complexity of these curved surfaces intrinsically induces self-shading and heterogeneous solar irradiation distribution. Crucially, the inherent geometric curvature dictates a continuous spatial variation in the solar incidence angle and equivalent irradiance. This phenomenon establishes pronounced irradiance gradients across the PV surface, which fundamentally alters the spatial distribution of photogenerated carriers and the subsequent electrical output. Consequently, this induces significant discrepancies in sub-unit current densities and exacerbates the risk of localized overheating. Ultimately, this complex photoelectric-thermal coupling and the resulting severe mismatch effects fundamentally threaten both system efficiency and operational reliability.

 doi:10.20944/preprints202604.0480.v1

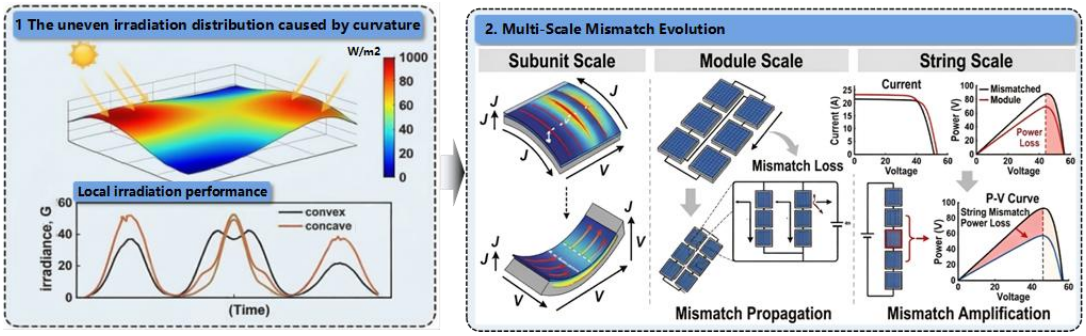

Figure 2. The Photoelectric mismatch mechanism.

Extensive research has investigated the mismatch effect in traditional planar PV systems, primarily focusing on discrete partial shading caused by adjacent obstacles, structural self-shading, or cloud cover. Zhao et al.[12] used ray tracing technology to achieve a coupled calculation of system-level shadow shading and mismatch losses. Saoud et al.[13] investigated the effect of partial shading on a complexly shaped c-Si based BIPV roof, optimizing for maximum yield to ascertain the optimal configuration and number of modules for each string using a genetic algorithm. Lu et al.[14] developed and validated a simulation model based on the double-diode model, systematically analyzing the impact of partial shading on concentrator photovoltaic (CPV) cell performance and revealing the nonlinear relationship between the geometric shading ratio and the effective irradiance loss. Zhang et al.[15] proposed a BD-ResVAE model that achieves high-accuracy bidirectional prediction between shading patterns and I-V curves. Li et al.[16] first proposed and validated a multiphysics model to predict the electrical, thermal, and structural performance of BIPV systems under non-shading, shading, and obstructed conditions simultaneously. It was revealed that hotspot-induced cell displacement (up to 0.85 mm) can exceed the compression range of the encapsulation material, leading to structural damage. Lance et al.[11] demonstrated that while curved modules can harvest up to 50% more irradiance than planar equivalents under the same 2D projected area, the dynamic shading on the curved surface generates complex, multi-peak power curves throughout the day. Similarly, Cai et al.[17] analyzed the mismatch losses in 2D and 3D curved silicon PV modules, revealing that optimizing cell interconnection strategies is crucial for mitigating these losses and enhancing power output.

To evaluate the performance of these complex geometries, numerous studies have relied on numerical modeling and validation experiments. For instance, Gong et al.[18] utilized EnergyPlus and Radiance software to simulate the performance of an arc-shaped CIGS window, determining the optimal central angle for building energy use intensity. Walker et al.[19] developed a parametric simulation workflow to calculate BIPV system losses using curved CIGS modules, identifying orientation dependencies. Tian et al.[20] compared the electrical performance of curved with flat CIGS PV modules under various meteorological conditions and tilt angles. The results showed that the flat module outperforms the curved one at a 30° tilt angle, with the performance gap decreasing as the tilt angle increases to 75°. The curved module exhibits a higher annual electricity especially at high inclination angles during the summer. Bugaj et al.[21] proposed a semi-flexible PVT system based on c-Si cells and use it to develop a testing methodology for various bendable conditions. The results indicated that when the bending angle modifier ranged from 1 to 1.1, the thermal power at a deflection of 30° was approximately 18% lower than that of the flat type, and the electrical power was nearly 14%. Yun et al.[22] introduced a curved honeycomb-structured Si PV module incorporating 3D mechanical metamaterials. By systematically harnessing additional reflected/scattered photons within its tetrahedral geometry, this structure demonstrated a 28% improvement in electrical output compared to flat type.

On the experimental front, controlled indoor tests have been predominantly utilized to assess baseline mechanical stability and steady-state electrical responses. Pei et al.[23] and Kashyap et al.[24] investigated the mechanical degradation and electrical parameters of flexible perovskite solar cells

 doi:10.20944/preprints202604.0480.v1

subjected to various concave, convex, and sinusoidal bending radii. Deepika et al.[25] investigated the performance of flexible perovskite solar cells under a 60° bending state, using a silica subwavelength array embedded on the substrate surface to optimize mechanical and optical performance. The results indicated that the current density increased by 7.30% when bent downwards and by 1.90% when bent upwards.

Although these fundamental indoor studies and numerical models can effectively clarify the optical laws and steady-state electrical characteristics, they are inherently limited in replicating the transient multi-physics coupling phenomena encountered in real outdoor applications. The physical curvature not only alters light absorption but fundamentally impacts local heat dissipation. Bugaj et al.[21] observed that bending a semi-flexible PVT structure by 30° resulted in an 18% reduction in thermal power and a nearly 14% drop in electrical output. Wang et al.[26] also highlighted the thermal-electrical dynamics in flexible CIGS curved PVT roofs for simultaneous electricity and hot water generation. However, a critical research gap persists regarding the component-level dynamic behavior of opaque, flexible PV modules operating strictly as exterior architectural envelopes under complex meteorological conditions. Unlike the stable environment of indoor simulators, continuous fluctuations in outdoor solar trajectories, ambient temperatures, and localized self-shading directly alter the activation sequence of bypass diodes, triggering highly dynamic mismatch phenomena. Furthermore, the localized thermal accumulation (hotspots) driven by these continuous irradiance gradients poses a severe threat to operational safety, yet it remains insufficiently quantified via in situ, high-resolution spatial mapping.

To bridge this fundamental gap, this paper presents a comprehensive outdoor experimental investigation focusing on the dynamic multi-physics response of opaque, flexible CIGS thin-film modules integrated onto curved geometries. Various typical building envelope bending forms were constructed, including length-convex (lgvx), length-concave (lgcv), width-convex (wdvx), width-concave (wdcv) , and length-wavy configurations. By deploying a full-scale outdoor testing platform in Hefei, China, this work meticulously captures the real-time electrical responses and simultaneously employs high-resolution infrared thermal imaging to monitor the spatiotemporal temperature distributions. The specific objectives are to elucidate the complex action mechanisms of bypass diodes under transient curved irradiance (manifested as multi-peak I-V curves) and to visually quantify the uneven thermal fields, thereby providing crucial empirical field data for the structural design and efficiency optimization of large-span curved BIPV roofs.

2. Experimental Setup and Methodology

To systematically investigate the complex mismatch mechanisms and localized thermal accumulations of curved BIPV systems under actual meteorological conditions, a comprehensive outdoor multi-physics testing platform was established on the rooftop of a building at the University of Science and Technology of China in Hefei (32° N, 117° E). This platform was specifically designed to capture the transient photoelectric-thermal coupling responses of full-scale flexible PV modules across various non-planar geometric configurations.

2.1. Module Configuration and Curved Surface Fabrication

To comprehensively evaluate the multi-peak current-voltage (I-V) characteristics induced by bypass diodes under continuous spatial irradiance gradients, commercial large-aspect-ratio flexible CIGS thin-film modules were selected for the full-scale experiments. The flat prototype module has dimensions of 1.72m in length and 0.35m in width, yielding an active power rating of 80W under Standard Test Conditions (STC).

Crucially, the internal electrical topology of the module was strictly documented to analyze the localized mismatch responses. As depicted in Fig.3, the module consists of 36 individual CIGS cell chips. To mitigate severe current mismatch losses, every four adjacent chips are parallel-connected to form a discrete sub-unit (chipset), and each sub-unit is bridged with a dedicated bypass diode. Consequently, the entire module comprises nine series-connected chipsets governed by nine

 doi:10.20944/preprints202604.0480.v1

corresponding bypass diodes. This precise electrical layout is the fundamental basis for the subsequent dynamic multi-peak I-V curve analysis under non-uniform illumination.The photoelectric specifications of the commercial PV module under standard testing conditions are listed in Table 1.

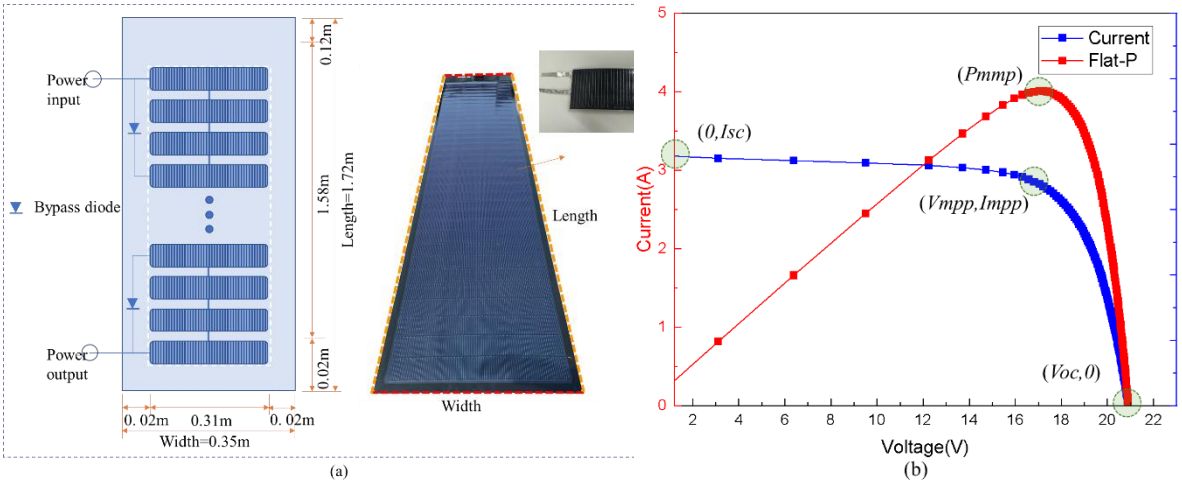

Figure 3. (a) The dimension of the flexible CIGS PV module; (b) I-V curve of the flat PV module(STC).

Table 1. Photoelectric specification of the flexible CIGS module under standard testing conditions.

Parameters	**Value (unit)**
Module length	1.72 m
Module width	0.35 m
PV chip numbers	36
Edge width	0.02m
Rated power at MPP (P_{mp})	80 W
Short current under STC (I_{sc})	4.74 A
Open voltage under STC (V_{oc})	23.8 V
MPP current under STC (I_{mp})	4.26 A
MPP voltage under STC (V_{mp})	18.8 V

To simulate typical curved architectural envelopes, precise mechanical fabrication was implemented. Aluminum baseplates were customized and formed into semi-cylindrical geometries (central angle of 180°) using a CNC press bending machine. The flexible CIGS modules were then conformally integrated onto these metallic substrates using highly conductive thermal silica gel. This metal-backed adhesive layer not only ensures structural integrity but also provides a realistic thermal dissipation boundary, distinct from the insulating properties of typical laboratory 3D-printed polymers. As illustrated in Fig. 4, six full-scale experimental configurations were established, including flat, length-convex, length-concave, width-convex, width-concave, and length-wavy profiles.

 doi:10.20944/preprints202604.0480.v1

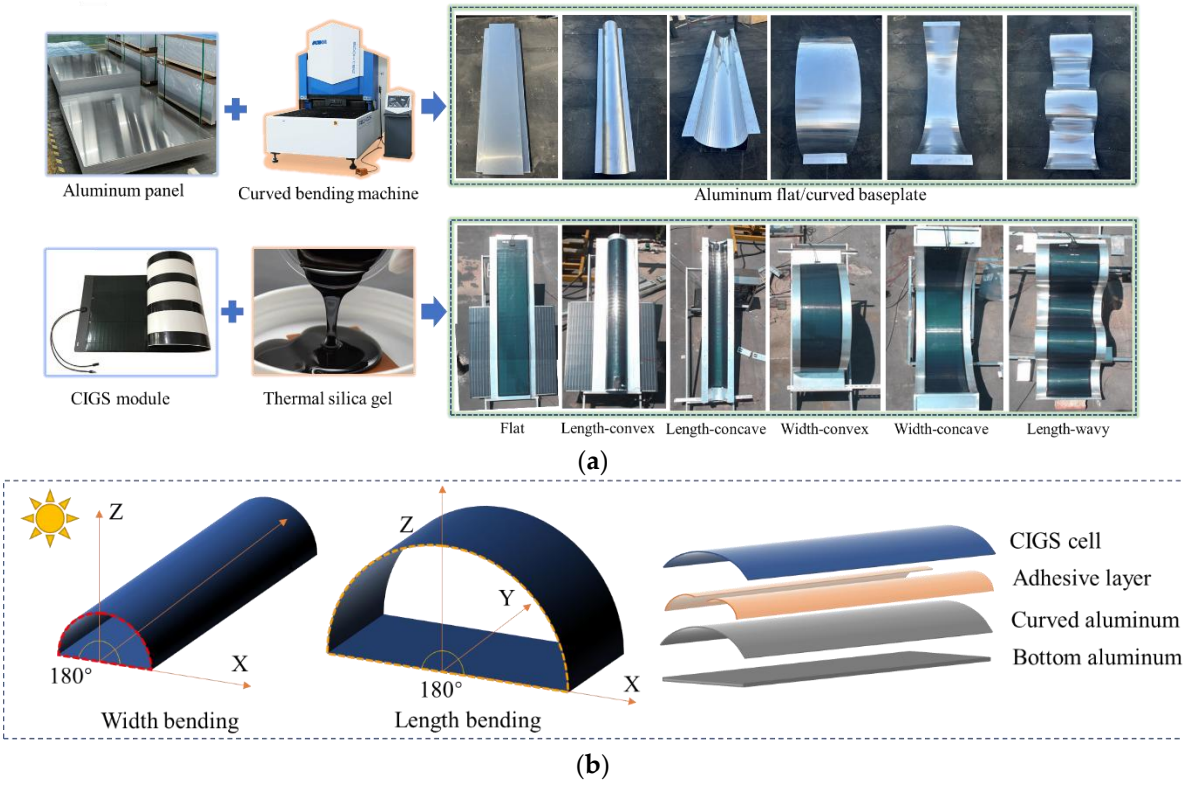

Figure 4. (a) The manufacturing process of the curved CIGS PV modules; (b) PV structure composition and two bending orientations.

2.2. The Outdoor Testing Contents and Apparatus

Real-world operation inherently exposes BIPV systems to transient solar irradiance, azimuth angle, and continuous ambient fluctuations. To accurately quantify these multi-physics variables, a synchronized data acquisition system was deployed. The schematic diagram of the complete workflow is shown in Fig.7.

Meteorological sensing: Real-time environmental parameters were continuously recorded at 10-second intervals using a high-precision data logger (HIOKI LR8402-21). Global solar irradiance on the inclined surface was measured by a TBQ-2 pyranometer, while diffuse irradiance was monitored by a horizontally mounted TBD-1 pyranometer equipped with a shading band. Ambient temperature and wind velocity were captured using a standardized louver box and a three-cup anemometer, respectively.

Electrical performance tracking: Each specific curved PV configuration was independently connected to a Maximum Power Point Tracking (MPPT) controller (EPEVER Tracer 1210AN), alongside direct current loads and storage batteries, forming a complete circuit. The instantaneous dynamic power output, operating voltage, and current were logged every 5 minutes utilizing eLOG01 data acquisition terminals. The detailed I-V characteristic curves were periodically scanned to capture the multi-peak phenomena triggered by bypass diode activation under non-uniform curved illumination.

Thermal field mapping: To evaluate the spatiotemporal temperature distributions and the evolution of localized hotspots driven by continuous irradiance gradients, continuous thermal monitoring was conducted. Discrete temperature measurements were obtained using calibrated T-type thermocouples symmetrically adhered to the rear surface of the modules (three points distributed along the longitudinal axis). Furthermore, a high-resolution infrared thermal imager (Fluke TiX1000) was employed during peak solar irradiance periods to quantitatively visualize the macroscopic uneven thermal fields across the curved PV surfaces. The related features are presented in Table 2.

 doi:10.20944/preprints202604.0480.v1

Table 2. Parameters of the experimental apparatus.

Content	Apparatus	Type	Accuracy
Solar irradiation	Pyranometer	TBQ-2	±2%
Temperatures	Thermocouple	T-type(copper-constantan)	±0.5℃
Wind velocity	Three-cup wind speed sensor	RS-FSJT-V10	±0.5m/s
Power output	MPPT & eLOG01	EPEVER Tracer 1210AN	±0.5%
Data switch unit	Datalogger	HIOKILR8402-21	±0.1%
Thermal image	Infrared thermal imager	Fluke TiX1000	±1.5℃

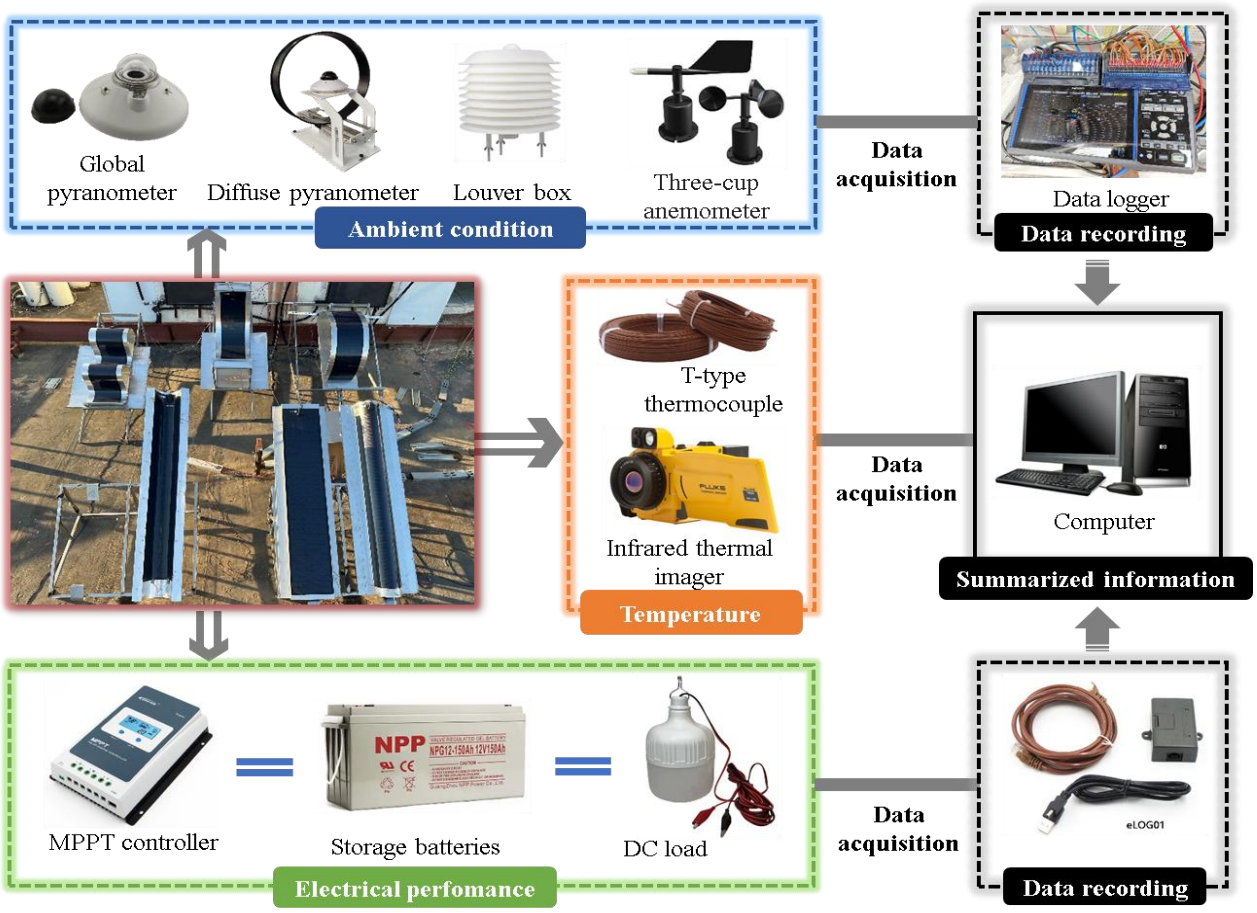

Figure 5. The schematic diagram of the complete workflow of the outdoor testing.

2.3. Performance Evaluation Metrics

To systematically quantify the dynamic degradation induced by the geometrical curvature and the subsequent mismatch effects, the comprehensive performance of the modules was evaluated using four critical indicators: the electrical efficiency, power mismatch loss, performance ratio, and fill factor.

(1) The electrical efficiency (η_{pv})

The definition of the electrical efficiency of the curved PV cells offers a good compromise between accuracy and simplicity, which has been studied in the authors' previous research[2, 3, 26].

 doi:10.20944/preprints202604.0480.v1

Therefore, this evaluation method is also defined as the ratio of the maximum power output to the incident solar energy on the orthographic projection area:

$$\eta_{pv} = \frac{P_{\max}}{G_{pv} A_{pv}} \times 100\% \quad (1)$$

Where: P_{max} is the instantaneous maximum power output of the PV module (W), G_{pv} *is* solar irradiation intensity on corresponding baseplate (W/m²), A_{pv} is the orthographic projection area of the curved PV module on inclined surface area (m²), the flat one is 0.49m², the curved ones are 0.35m² .

(2) Power mismatch loss (ΔP_{ml})

The mismatch loss in the curved PV cells/modules can be defined as the difference between the power output of a flat PV and a curved one with the same specifications[17].The mismatch loss can be defined as:

$$\Delta P_{ml} = P_{flt} - P_{crv} \quad (2)$$

Where, P_{flt} is the flat type PV power output; P_{crv} is the curved type PV power output.

(3) Performance ratio (PR)

In this study, performance ratio is defined as the ratio of the power output of the curved PV to the flat PV with the same specifications, which is given below:

$$PR = \frac{P_{crv}}{P_{flt}} \times 100\% \quad (3)$$

(4) Filling factor (FF)

The filling factor is an inevitable parameter to describe the performance of PVs under partial shadings. FF is defined as the ratio of the actual maximum power output of the PV cells/modules to the rated maximum power output. The higher the value, the higher the photoelectric conversion efficiency. The formula is:

$$FF = \frac{P_{\max}}{V_{oc} I_{sc}} \quad (4)$$

Where: V_{oc} is the open circuit voltage (V); I_{sc} is the short circuit current (A);

2.4. Uncertainty Analysis

Uncertainty analysis is essential in experimental studies to establish credibility and reliability in the results[28]. The systematic uncertainties originated primarily from the measuring instruments, including the pyranometers, T-type thermocouples, and the MPPT data acquisition system. Assuming a uniform probability distribution, the standard uncertainty of each instrument (u_B) is calculated by Eq. (5)[29]:

$$u_B = \frac{a_n}{\sqrt{3}} \quad (5)$$

Where a_n is the nominal accuracy of the experimental instrument provided by the manufacturer (as detailed in Table 3).

The combined standard uncertainty u_c is determined using Eq. (6), which is calculated based on the standard uncertainties of the measurement devices utilized.

$$u_c = \sqrt{\sum u_B^{\,2}} \quad (6)$$

Based on the standard uncertainties of the measurement devices utilized, the maximum total uncertainty of this outdoor experiment is quantified as 1.70%, ensuring the validity of the results.

Table 3. Parameters of the measuring instruments used in the experiment.

 doi:10.20944/preprints202604.0480.v1

Instrument name	Test content	Type	Accuracy	Uncertainty
Solar global pyranometer	Global irradiance	Jinzhou TBQ-2	± 2%	1.15%
Solar diffuse pyranometer	Diffuse irradiance	Jinzhou TBD-1	± 2%	1.15%
Thermocouple	Temperature	T-type (copper-constantan)	± 0.5℃	0.29%
MPPT controller	Electrical power	EPEVER Tracer 1210AN	± 0.5%	0.29%
Datalogger	Data switch unit	HIOKI LR8402-21	/	/

3. Results and Discussions

Operating BIPV systems in actual outdoor environments introduces transient meteorological variables that cannot be fully replicated in steady-state indoor simulators. This section systematically evaluates the dynamic electrical degradation and multi-physics coupling effects of the full-scale curved flexible CIGS modules under continuous spatiotemporal irradiance gradients.

3.1. Transient Meteorological Conditions

As depicted in Fig.6, the tests lasted from the initial low irradiance to the highest irradiance, then till the irradiance decreased, describing convincible results. To ensure a rigorous comparative analysis, the outdoor experimental data selected for discussion were collected during typical clear-sky sunny days in July 2024. The ambient conditions inherently dictated the transient multi-physics boundary for the PV modules. The highest irradiance of the days can be over 1000W/m2 at around 12:00 PM. For the longitude oriented configurations, the ambient temperature fluctuated between 32.8°C and 36.7°C, with a total daily solar irradiation of 9.12 MJ. Correspondingly, the latitude configurations experienced slightly harsher thermal conditions, with ambient temperatures ranging from 33.6°C to 41.0°C and a total irradiation of 9.17 MJ. These high-irradiance and high-temperature conditions perfectly exposed the vulnerability of curved modules to photoelectric mismatch and localized thermal accumulations.

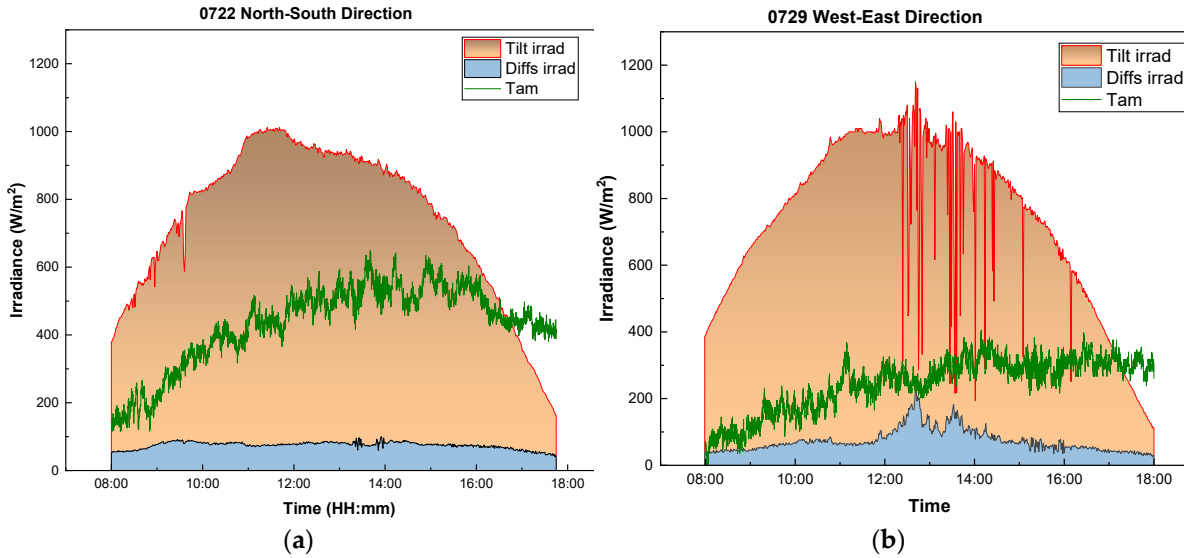

Figure 6. Ambient conditions of the experiments in July, 2024.

3.2. Dynamic Electrical Performance and Multi-Peak I-V Characteristics

 doi:10.20944/preprints202604.0480.v1

As illustrated in Fig.7a-b, the flat-type PV module exhibited the best electrical power output for the majority of the time, reaching a peak of over 70 W at noon due to the absence of the mismatch phenomenon. In contrast, the wy bending form manifested the poorest performance. The power loss gap between the width-curve type and flat type was smaller than that between the length-curve and flat type. However, an interesting inversion occurs in the early morning and late afternoon, where the wdvx configurations in the longitude direction actually outperformed the flat-type. The wdvx shapes demonstrated the electrical efficiency ranged 11.00%-23.00%, the flat-typed shapes ranged 6.50%-15.50%, the lgvx shapes ranged 6.00%-10.50%, the lgcv shapes ranged 4.10%-11.00%, the wdcv shapes ranged 3.00%-12.50%. Among the width-bending forms, the electrical efficiency curves of wdvx configurations were presented like an "U" shaped, while others are presented like an upside-down "U", which is similer to the irradiance changes.

As illustrated in Fig.7c-d, the wdvx shapes in longitude direction reached the highest efficiency point, the wy configurations produced the lowest point. It was observed that the electrical efficiency of wy shapes or lgcv shapes changed fluctuatly. Notably, the lgvx in latitude direction demonstrated higher electrical efficiency than that in the longitude direction. Conversly, the wdvx in the longitude direction produced higher electrical efficiency than in the latitude direction.

In the width-bending configurations, the convex configurations received a greater amount of irradiance compared to the concave ones. This can be attributed to the fact that the short side of the bending symmetrically forms two upward-facing segments. The self-shadowing of the shape has a more significant impact on the electrical performance than the reflection of solar irradiance between the two erected parts. During the early morning and late afternoon, the convex configurations demonstrate optimal electrical performance as their two sides receive solar irradiance more directly than others. For length-bending configurations, due to the partial shadow cast by the sun on the shapes, the shadow area changes concurrently. Consequently, the solar irradiance distribution of the curved PV modules is variable, leading to different values of power output and electrical efficiency.

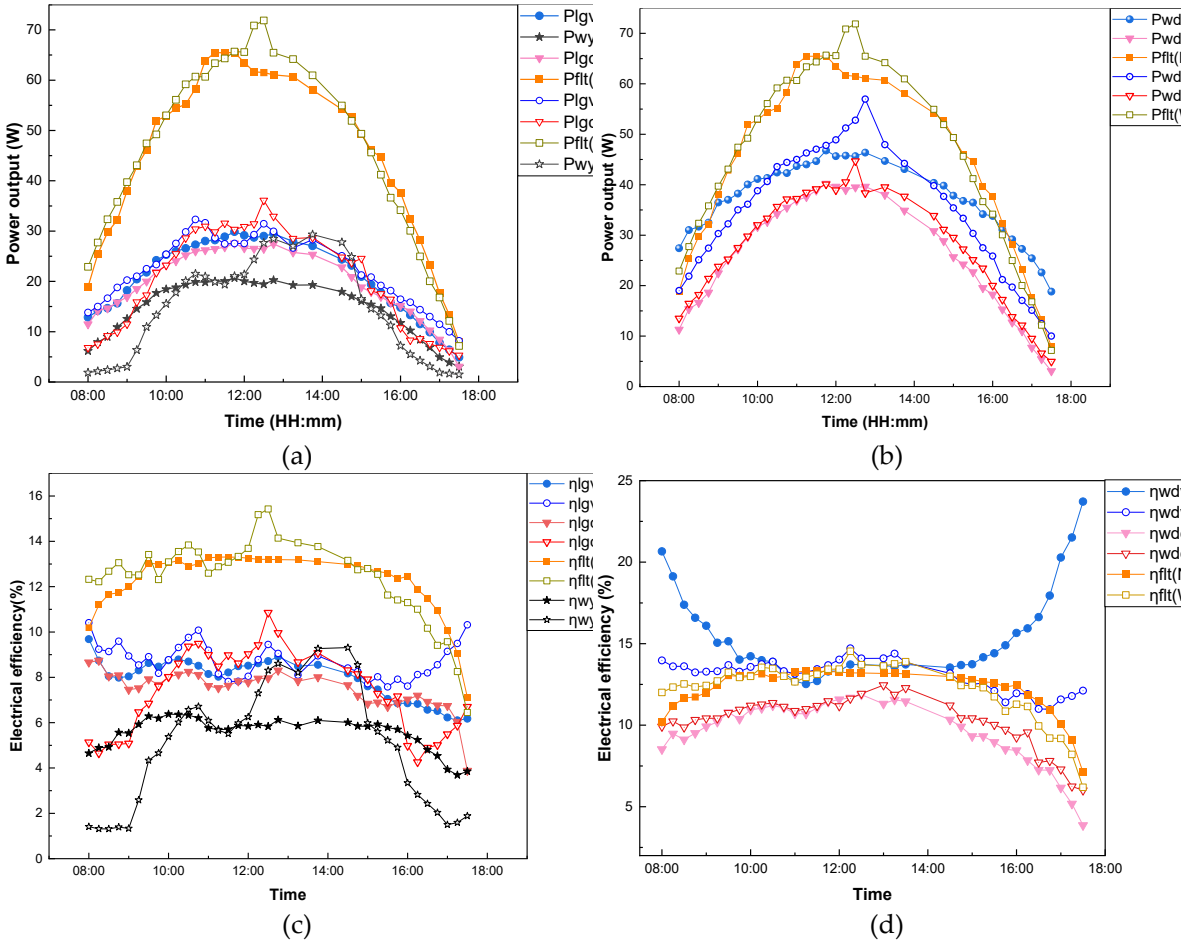

 doi:10.20944/preprints202604.0480.v1

Figure 7. Electrical performance of the curved PV modules.

As illustrated in Fig.8, the flat-type module exhibited a smooth, standard single-peak curve, confirming the absence of spatial mismatch. Among the curved configurations, the wdvx shapes in both orientations demonstrated minimal mismatch severity; their I-V curves remained relatively smooth, indicating that the irradiance gradient along the short axis did not severely trigger the bypass diodes. Conversely, the wdcv shapes manifested distinct double-trough characteristics, with current decreasing sharply as voltage increased. More critically, the lgcv and lgvx configurations exhibited a severe step-like degradation in current, resulting in multiple peaks and troughs during the tests.

As the transient solar trajectory cast continuous, localized self-shading across the long axis of the module, the individual parallel-connected chipsets operated under drastically different localized irradiances. The severely shaded chipsets became reverse-biased, forcing their corresponding bypass diodes into conduction to prevent hotspot failure, thereby bypassing that entire sub-unit's power contribution and creating the distinct multiple peaks on the I-V curve.

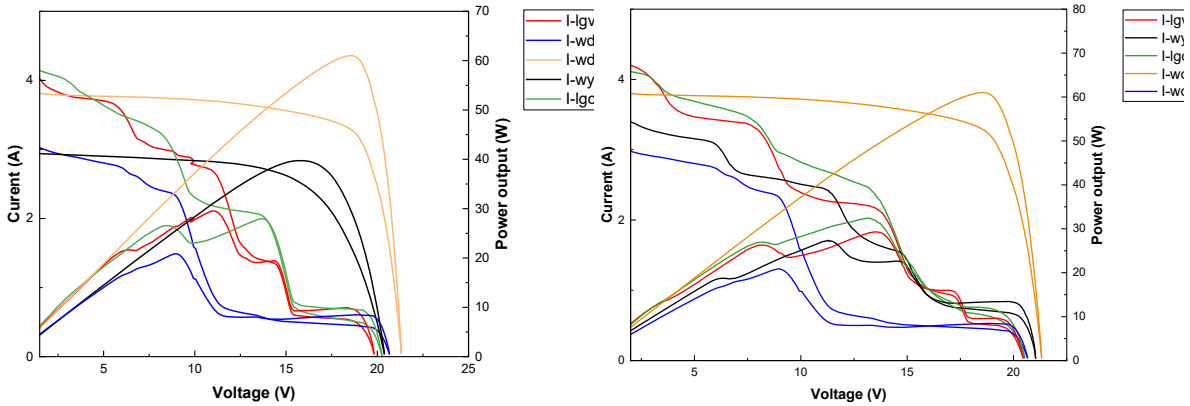

(a) (b)

Figure 8. The I-V curve of the PV modules at 12:00PM.

3.3. Daily Energy Yield and Efficiency Degradation

The power output of PV modules with different shapes varied every seconds, and the daily electrical yield exhibited certain regular patterns. As illustrated in Fig.9, the highest total power output during the tests is the flat-type, reaching 453.32Wh. Obviously, the different shapes presented a decreasing trend in both longitudinal direction and latitudinal direction, regardless of their varying behavior during the tests. Arranged these groups of data in both directions from high to low, the order is: flat > wdvx > wdcv > lgvx > lgcv > wy. Besides, the average electrical efficiency changes as the decreasing trend of daily electricity yield. Notably, the average electrical efficiency and fill factor of the wdvx shapes reached their peak values. This can be attributed to the fact that, the wdvx shapes didn't exhibited much mismatch loss and have great potential in curved BIPV applications than the flat type ones.

 doi:10.20944/preprints202604.0480.v1

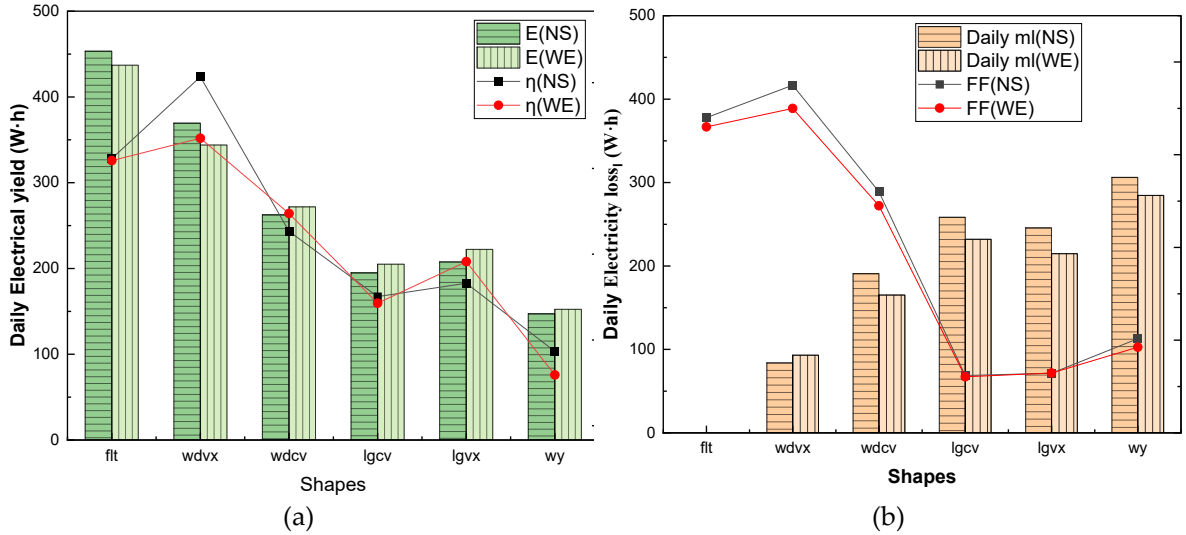

Figure 9. Daily electrical yield and mismatch loss.

The specific mismatch losses and performance ratios(PR) for all distinct 11 shapes including longitudinal and latitudinal placements were presented in Fig.10. It can be clearly observed that the mismatch loss of each configuration exhibited symmetric changes. In comparison to the width-bending configurations, the length-bending ones demonstrated greater mismatch losses. Notably, only the convex-shaped forms showed positive power output in the early morning and late afternoon of a day. The mismatch loss varied as the solar irradiance changed. A pronounced effect consistently occurred at noon when the solar irradiance was at its peak, while the effect was less significant during the morning and at sunset. Among all configurations, the wdvxs exhibited the least power loss; conversely, the wy shapes had the highest power loss. The Performance Ratio (PR) increased as the bending shapes changed, following a pattern similar to that of the power output. From low to high, the order is as follows: wdvx(WE) > wdvx(NS) > wdcv(NS) > wdcv(WE) > lgvx(NS) > lgvx(WE) > lgcv(NS) > lgcv(WE) > wy (NS) > wy(WE). The wy configurations in the latitudinal direction have the lowest average PR of 27.22%, while the wdvx configurations in the longitudinal direction exhibit the highest average PR of 91.46%.

Notably, an inversion in geometric performance superiority occurred outdoors compared to typical indoor assumptions. This is attributed to the macroscopic convex morphology forming upward-facing segments that directly capture a broader solid angle of solar radiation, whereas the concave structure suffers from severe structural self-shading that outweighs any marginal internal reflection gains.

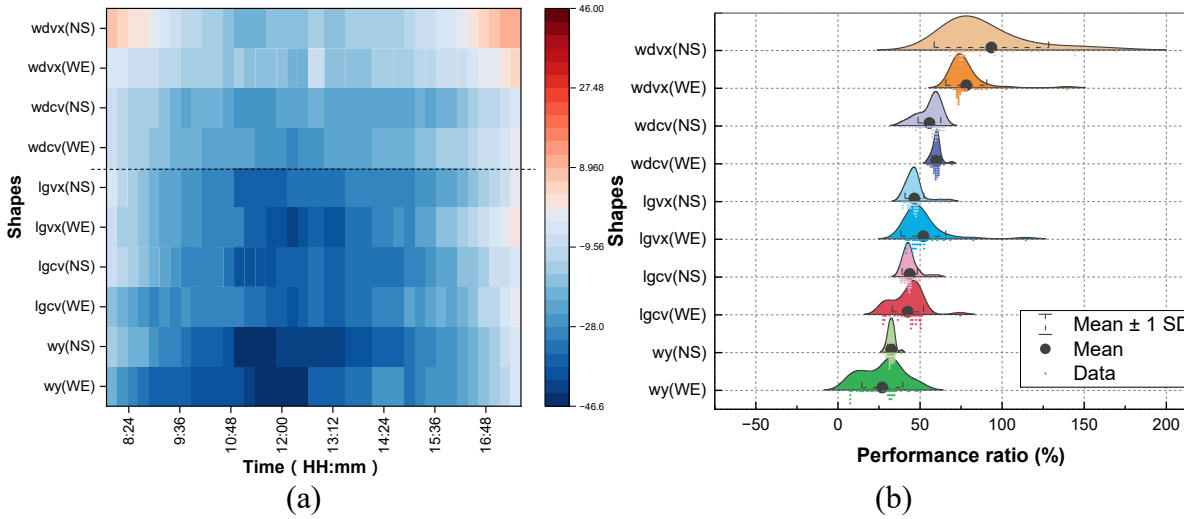

 doi:10.20944/preprints202604.0480.v1

Figure 10. The mismatch loss and performance ratio of the PV modules.

3.4. Thermal Distribution and Localized Hotspot Evolution

Beyond electrical degradation, the continuous irradiance gradients on curved BIPV surfaces induce localized thermal accumulations. As shown in Fig. 11, the temperature of the length-bending shapes was consistently higher than that of the width-bending ones. The lgcv(NS) configurations exhibited the highest peak temperature, reaching 65.88°C. Generally, temperature changes followed the solar irradiance and were influenced by the electrical efficiency. In the morning, with solar irradiation originate from the east, the west side of the curved module may lack direct exposure. In the afternoon, the east side has the same issue as the sun moves west.

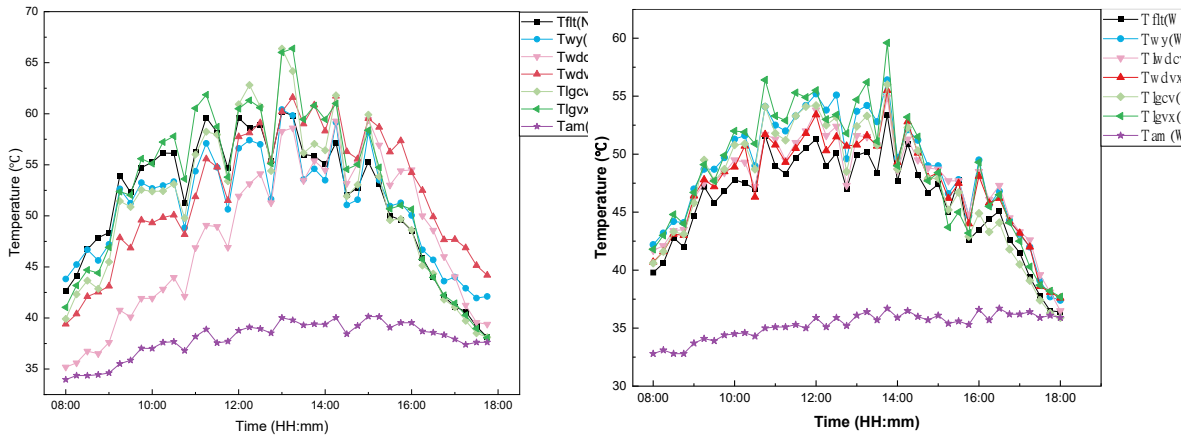

Figure 11. The temperature distribution of the curved PV modules.

As presented in Fig.12, high-resolution infrared thermal imaging vividly quantified this thermal-electrical coupling. The temperature distribution of each curved shape was symmetric, with the highest values consistently occurring at the middle of the modules. The flat-type module exhibited a highly uniform temperature distribution across its entire surface, verifying homogenous solar absorption. For width-bending configurations, lower temperatures were found on the west and east side, whereas for length-bending configurations, the lower temperatures were on the north and south side. This spatiotemporal non-uniformity highlights how dynamic solar azimuth and localized structural self-shading drive significant thermal gradients.

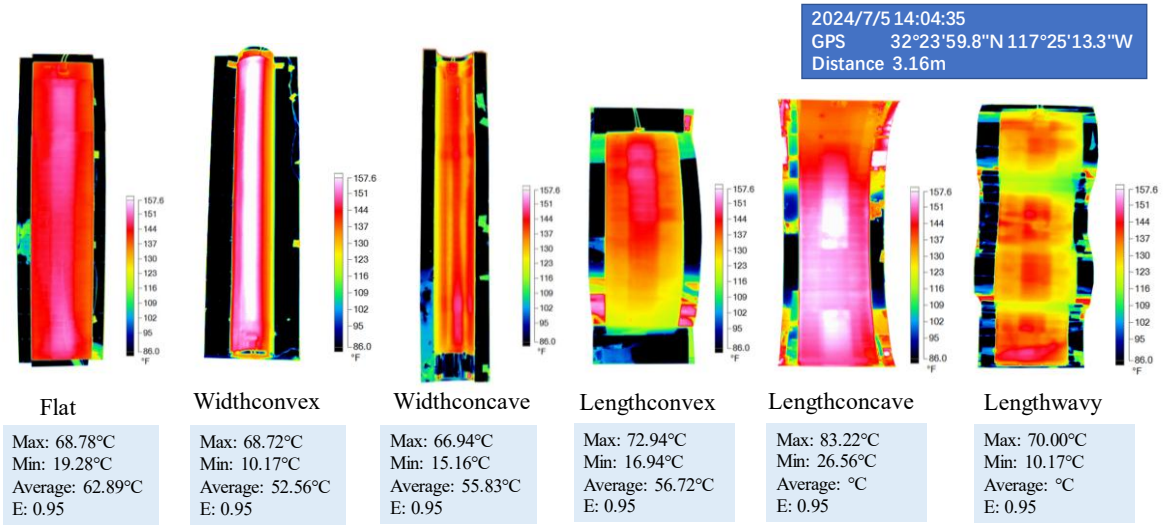

Figure 12. The infare thermal image of the curved PV modules.

 doi:10.20944/preprints202604.0480.v1

4. Conclusions

The widespread application of flexible CIGS thin-film modules on large-span architectural envelopes necessitates a deep understanding of their dynamic behavior under complex geometric and meteorological boundary conditions. Moving beyond conventional steady-state indoor testing, this study established a full-scale outdoor multi-physics experimental platform to systematically quantify the transient photoelectric-thermal coupling and mismatch mechanisms of opaque, curved BIPV modules. The principal conclusions are as follows:

(1) **Severe dynamic electrical mismatch and multi-peak phenomena:** Continuous spatial curvature intrinsically generates severe irradiance gradients. Under real-world transient solar trajectories, this non-uniformity triggers the sequential, dynamic activation of bypass diodes across parallel-connected chipsets, fundamentally altering the internal electrical topology and resulting in severe step-wise current constraints and multi-peak I-V characteristic curves.

(2) **Geometric dependency of power degradation:** The energy yield and performance ratio (PR) are strictly governed by the macroscopic geometric curvature. Throughout a typical clear-sky operating day, the electrical performance follows a distinct hierarchical decline: flat > width-convex > width-concave > length-convex > length-concave > length-wavy. Notably, due to the advantageous upward-facing morphological segments, width-convex configurations demonstrate significantly higher resilience to outdoor mismatch losses compared to concave counterparts. The average power output of different bending forms decreased by 54.45% of length-convex(NS) shapes, 56.24% of length-concave(NS) shapes,67.60% of length-wavy(NS) shapes, 6.53% of wdvx-convex(NS) shapes, 45.26% of width-concave(NS) shapes.

(3) **Localized thermal accumulation risks:** High-resolution infrared thermography vividly demonstrated that geometric self-shading and continuous irradiance gradients induce profound spatial temperature non-uniformity. The un-converted optical energy in localized shaded regions translates into extreme thermal hotspots, exacerbating photoelectric efficiency drops and threatening the long-term operational durability of the BIPV array.

(4) **Engineering implications for curved BIPV:** The experimental evidence underscores that applying standard planar PV interconnection logic to curved surfaces is highly detrimental. To ensure system reliability and optimize energy yield, future large-scale curved BIPV roofs require customized, high-granularity series-parallel topological designs (or module-level power electronics such as micro-inverters) tailored to specific architectural curvatures, coupled with highly conductive metallic substrates to mitigate localized thermal stress.

Nomenclature

A_c	the overall area of the orthographic projection of eight curved PV/T units on the inclined surface, m²	P_{max}	the instantaneous maximum power output of the PV module,W
G_{pv}	Solar irradiation intensity on baseplate,W/m²	A_{pv}	the orthographic projection area on inclined surface area,m²
η_{pv}	Electrical efficiency,%	P_{flt}	The flat type PV power output,W
ΔP_{ml}	Power mismatch loss,W	P_{crv}	The curved type PV power output,W
PR	Performance ratio,%	FF	Filling factor
Voc	The open circuit,V	Isc	The short current,A
u_B	The standard uncertainty of the instruments	a_n	The nominal accuracy of the experimental instrument
u_c	The uncertainty		

 doi:10.20944/preprints202604.0480.v1

Author Contributions: Conceptualization, **Jun Wang** and **Xinyi Tian**; methodology, **Jun Wang** and **Xinyi Tian**; software, **Mingjun Jiang**; validation, **Guodong Lu**; formal analysis, **Jun Wang, Xinyi Tian, Jie Ji**; investigation, **Jun Wang, Mingjun Jiang, Guodong Lu**; resources, **Qiansheng Fang, Haitao Wang**; data curation, **Mingjun Jiang**; writing—original draft preparation, **Jun Wang**; writing—review and editing, **Jun Wang, Xinyi Tian, Jie Ji**; visualization, **Guodong Lu**; supervision, **Jie Ji, Qiansheng Fang**; project administration, **Jie Ji, Qiansheng Fang, Haitao Wang**; funding acquisition, **Jie Ji, Qiansheng Fang.** All authors have read and agreed to the published version of the manuscript.

Conflicts of interest: The authors declare no conflict of interest.

Acknowledgments: This research was funded by [**National Key Research and Development Project**] grant number [No.2023YFC3807704, No.2022YFB4201002], [**National Natural Science Foundation of China**] grant number [No.52238004] , [**Anhui Provincial Department of Education Natural Science Key Project**] grant number [2024AH050233], [**Anhui Jianzhu University Research Project**] grant number [2024QDHZ09]. The APC was funded by [**No.2023YFC3807704**]. Information regarding the funder and the funding number should be provided. Please check the accuracy of funding data and any other information carefully.

References

1. CABEE. 2025 China's Carbon Emission Report on Urban and Rural Construction. 北京 2026.
2. Tian X, Wang J, Ji J, Xia T. Comparative performance analysis of the flexible flat/curved PV modules with changing inclination angles. Energy Conversion and Management. 2022;274.
3. Wang J, Tian X, Ji J, Xie H, Yuan S. A comparative study on curved air-based photovoltaic/thermal roofs with and without glazing. Applied Thermal Engineering. 2023;219.
4. Hu Z, Zhang S, Hou J, He W, Liu X, Yu C, et al. An experimental and numerical analysis of a novel water blind-Trombe wall system. Energy Conversion and Management. 2020;205.
5. Su X, Luo C, Chen X, Jiang Q, Yu Y, El Shenawy ET, et al. Experimental and theoretical analysis of photovoltaic performance and thermal behavior for bifacial PV-Trombe wall system with reversible louvers in summer. Energy. 2024;312.
6. Zhang C, Ji J, Wang C, Ke W, Xie H, Yu B. Experimental and numerical studies on the thermal and electrical performance of a CdTe ventilated window integrated with vacuum glazing. Energy. 2022;244.
7. Shi S, Zhu N, Li Y, Song Y. Photo-thermal decoupling CdTe PV windows with selectively near-infrared absorbing ATO nanofluids. Renewable Energy. 2024;235.
8. Meng Y, Tan Y, Li X, Cai Y, Peng J, Long Y. Building-integrated photovoltaic smart window with energy generation and conservation. Applied Energy. 2022;324.
9. M. Krarti AK. Evaluation of static and dynamic PV-Integrated shading systems for office spaces in Australia. Solar Energy. 2024;277(112736).
10. Li X, Peng J, Li N, Wu Y, Fang Y, Li T, et al. Optimal design of photovoltaic shading systems for multi-story buildings. Journal of Cleaner Production. 2019;220:1024-38.
11. Balog LARS. Energy harvest potential of flexible photovoltaics on curved surfaces. IEEE. 2019.
12. Zhao C, Xiao J, Yu Y, Jaubert J-N. Accurate shading factor and mismatch loss analysis of bifacial HSAT systems through ray-tracing modeling. Solar Energy Advances. 2021;1.
13. Al-Janahi SA, Ellabban O, Al-Ghamdi SG. A Novel BIPV Reconfiguration Algorithm for Maximum Power Generation under Partial Shading. Energies. 2020;13(17).
14. Lu Y, Wang L, Wang J, Liu P, Rafee R, Rashidi S, et al. Effect of partial shading on the performance of concentrated photovoltaics: a simulation and experimental study based on the double-diode model. Energy. 2026;348.
15. Zhang C, Yu Y, Yang Z, Cao K, Huang H, Gao Q, et al. Multiscale analysis and deep learning-based prediction of partial shading for TBC and TOPCon PV modules. Renewable Energy. 2026;266.
16. Li Q, Zhu L, Sun Y, Lu L, Yang Y. Performance prediction of Building Integrated Photovoltaics under no-shading, shading and masking conditions using a multi-physics model. Energy. 2020;213.

 doi:10.20944/preprints202604.0480.v1

17. Cai J, Fang J, Liang M, Zhu Q, Shi Z, Li Q, et al. Dynamic performance enhancement in 2D and 3D curved flexible photovoltaic modules: Mismatch loss analysis and cell interconnection configurations optimization. Applied Energy. 2024;374.
18. Gong F, Gao Y, Tian X, Wang J, Ji J, Shi F, et al. Simulation of a novel curved photovoltaic (PV) window improving the annual daylighting and building energy performance simultaneously. Building Simulation. 2024;17(11):1951-69.
19. Walker L, Hofer J, Schlueter A. High-resolution, parametric BIPV and electrical systems modeling and design. Applied Energy. 2019;238:164-79.
20. Tian X, Wang J, Ji J, Lu G. The performance investigation of the flexible photovoltaic cell under non-uniform distributed illumination. Renewable Energy. 2025;240.
21. Bugaj MA, Mik K. Can PVT bend?: The elaboration of flexible hybrid photovoltaic thermal solar collector structure and testing methodology. Renewable Energy. 2023;215.
22. Yun MJ, Sim YH, Lee DY, Cha SI. Honeycomb--Structured 3D Concave Photovoltaic Modules Supported by 3D Mechanical Metamaterials for Enhanced Light Recapture. Advanced Materials Technologies. 2022;8(2).
23. Pei L, Yu H, Zhang Q, Li J, Wang K, Hu B. Concave and Convex Bending Influenced Mechanical Stability in Flexible Perovskite Solar Cells. The Journal of Physical Chemistry C. 2020;124(4):2340-5.
24. Kashyap S, Pandey R, Madan J, Mohammed MKA. Reliability Test of 21% Efficient Flexible Perovskite Solar Cell Under Concave, Convex and Sinusoidal Bending. IEEE Transactions on Device and Materials Reliability. 2023;23(3):380-5.
25. Deepika, Singh A, Verma UK, Tonk A. Device Structures of Perovskite Solar Cells: A Critical Review. physica status solidi (a). 2023;220(9).
26. Wang J, Tian X, Ji J, Zhang C, Ke W, Yuan S. Field experimental investigation of a multifunctional curved CIGS photovoltaic/thermal (PV/T) roof system for traditional Chinese buildings. Energy Conversion and Management. 2022;271.
27. Ma T, Guo Z, Shen L, Liu X, Chen Z, Zhou Y, et al. Performance modelling of photovoltaic modules under actual operating conditions considering loss mechanism and energy distribution. Applied Energy. 2021;298.
28. Agyekum EB, PraveenKumar S, Alwan NT, Velkin VI, Shcheklein SE, Yaqoob SJ. Experimental Investigation of the Effect of a Combination of Active and Passive Cooling Mechanism on the Thermal Characteristics and Efficiency of Solar PV Module. Inventions2021.
29. Alwan NT, Majeed MH, Shcheklein SE, Ali OM, PraveenKumar S. Experimental Study of a Tilt Single Slope Solar Still Integrated with Aluminum Condensate Plate. Inventions2021.